Atmos. Chem. Phys. Discuss., 3, 3301–3333, 2003
www.atmos-chem-phys.org/acpd/3/3301/

Atmospheric Chemistry and Physics Discussions

Cirrus cloud occurrence as function of ambient relative humidity: A comparison of observations from the Southern and Northern Hemisphere midlatitudes obtained during the INCA experiment

J. Ström[1], M. Seifert[1], B. Kärcher[2], J. Ovarlez[3], A. Minikin[2], J. F. Gayet[4], R. Krejci[1], A. Petzold[2], F. Auriol[4], R. Busen[2], U. Schumann[2], W. Haag[2], and H. C. Hansson[1]

[1]ITM, Air Pollution Laboratory, Stockholm University, Sweden
[2]DLR, Institut für Physik der Atmosphäre, Oberpfaffenhofen, Germany
[3]LMD, Ecole Polytechnique, Palaiseau, France
[4]LAMP, Université Blaise Pascal, Aubiére, France

Received: 24 March 2003 – Accepted: 20 June 2003 – Published: 30 June 2003

Correspondence to: J. Ström (johan@itm.su.se)

Abstract

The occurrence frequency of cirrus clouds as function of ambient relative humidity over ice, based on in-situ observations performed during the INCA experiment, show a clear difference between the campaign carried out at Southern Hemisphere (SH) midlatitudes and the campaign carried out at Northern Hemisphere (NH) midlatitudes. At a given relative humidity above ice saturation, clouds are more frequent in the NH. At relative humidities near ice saturation, clouds defined as containing particles with sizes larger than 0.55μm diameter and an integral number density above 0.2 cm^{-3} were present 70% of the time during the SH campaign, whereas clouds where present 95% of the time during the NH campaign. Using a size threshold of 1 μm diameter to define the presence of clouds result in a less frequent occurrence of 60% of the time in the SH campaign and 75% of the time in the NH campaign. The data show that the presence of particles is a common characteristic of cirrus clouds. Clouds at ice saturation defined as having crystal sizes of at least 5μm diameter and a number density exceeding 0.001 cm^{-3} were present in about 80% of the time during the SH campaign, and almost 90% of the time during the NH campaign. The observations reveal a significant cloud presence fraction at humidities well below ice saturation. Local minima in the cloud presence fraction as a function of relative humidity are interpreted as systematic underestimation of cloud presence because cloud particles may become invisible to cloud probes. Based on this interpretation the data suggests that clouds in the SH form preferentially at relative humidities between 140 and 155%, whereas clouds in the NH formed at relative humidities less than 130%. A simple assumption about the probability to reach successively higher humidities in an ice supersaturated air parcel provides a model that explains the main trend of the cloud presence fraction as function of relative humidity. If adiabatic processes are assumed a cloud water content distribution can be derived from this probability model. The resulting distribution agrees well in shape compared to observations, but the observed mean cloud water content is less than expected from simply adiabatic processes.

1 Introduction

There is a concern that anthropogenic emissions may change the environment in a way that it could influence the frequency of occurrence and microphysical properties of cirrus clouds. An obvious anthropogenic modification of the cloud frequency of occurrence is condensation trails formed behind aircraft near the tropopause. Based on analyzed satellite data from 1996 and 1997, Mannstein et al. (1999) and Meyer et al. (2002) deduced that linear persistent contrails cover about 0.5–0.7% of the sky at noon over Europe in the annual average. These results exemplify the possible regional effect by contrails. Although the effect by contrails may be noticeable on a regional scale it is currently estimated to have a small (IPCC 1999, EC 2002) effect on the global climate.

Besides this direct contrail effect there are observations indicating that indirect aerosol effects may influence the properties of high clouds as well (Ström and Ohlsson, 1998; Boucher, 1999; Kristensson et al., 2000). Numerical simulations using freezing rates based on recent laboratory measurements suggest that the effect from changes in ambient sulfate aerosol properties may have a marginal effect on the microphysical properties and lifecycle of cirrus (Lohmann and Kärcher, 2002; Kärcher and Lohmann, 2002). A pronounced indirect aerosol effect on cirrus is possible when at least two types of freezing aerosol particles compete during cloud formation (Kärcher and Lohmann, 2003): adding efficient ice nuclei to liquid sulfate aerosols can lead to a marked suppression of pristine ice crystal number densities, the magnitude of this effect depending on updraft speed, temperature, and number and freezing properties of the ice nuclei.

Compared to our current level of understanding about warm clouds, fundamental knowledge about cirrus formation is still lacking, and there are still open issues regarding the preferred mode of ice nucleation (homogenous vs. heterogeneous), and the typical number densities and size of ice crystals in cirrus clouds. The situation is complicated by the fact that the efficiency with which aerosol particles freezes is strongly linked to the dynamical conditions prevailing during ice formation (Kärcher and Ström,

2003).

Studying a possible anthropogenic effect on high clouds involve detecting a subtle but systematic difference between the properties of clouds formed in a pristine environment to those formed in a perturbed environment. The possible anthropogenic influence on warm clouds has been studied extensively and covers just about every type of environment present in both hemispheres. However, until recently all in-situ measurements of midlatitude cirrus had been performed in the Northern Hemisphere. With the project INCA (Interhemispheric differences in cirrus properties from anthropogenic emissions) the first observations of cirrus properties in the Southern Hemisphere midlatitudes became available that allow the comparison of clouds formed in two very different regions of the world under comparable meteorological conditions.

In the year 2000, two aircraft campaigns were performed as part of INCA, one in the Southern Hemisphere (SH) and one in the Northern Hemisphere (NH) midlatitudes. Here the abbreviations, SH and NH, are used to identify the different campaigns and do not refer to hemispherically averaged properties. The first campaign based in Punta Arenas, Chile (54° S) was performed in March and April. The second campaign based in Prestwick, Scotland (55° N) was performed in September and October. Hence, the campaigns were performed in equivalent seasons. For more information about the INCA experiment we refer to: http://www.pa.op.dlr.de/inca/.

One of the first results presented from the INCA experiment was a comparison of relative humidity distributions observed during the two campaigns (Ovarlez et al., 2002). Both data sets presented a maximum in the frequency distribution around 100% with respect to ice (RHI), but the distribution was skewed towards higher humidities in the SH data. This observed difference in relative humidity distributions raised an interesting question regarding cirrus properties. If the distributions of relative humidity were different, would this also be reflected in the cloud occurrence frequency? The present work compares the occurrence of clouds as function of relative humidity observed during the two campaigns.

Although a cloud is something known to everyone, it may sometimes be difficult or

even impossible to provide a simple definition for when a cloud is actually present or not. What is the minimum crystal number density or horizontal and vertical extent necessary for an ensemble of hydrometeors to be called a cloud? Is a 1 m thick layer or a particle number density of 1 m^{-3} sufficient? We can raise similar questions for any observable parameter determined by in-situ or remote sensing methods alike. Because of theses difficulties the presence or non-presence of a cloud is usually determined by the detection limit of the particular sensor used to observe the cloud. What is interpreted as a cloud by one sensor might be interpreted as cloud-free air by another. In this study we will make use of four different cloud sensors to investigate the presence or non-presence of cirrus clouds as function of ambient relative humidity. These instruments are the Counterflow Virtual Impactor (CVI), the PMS FSSP-300, the PMS 2D-probe, and the Polar Nephelometer. The same instruments were used in both campaigns, which permit a direct comparison of the observations with respect to an unchanged payload configuration.

2 Methodology

We define the cloud presence fraction (CPF) as the ratio between the number of data points determined to be cloud at a given relative humidity over ice (RHI) divided by the total number of observations at that relative humidity. To determine the presence or non-presence of cloud we make use of data from the Counterflow Virtual Impactor (CVI), the PMS FSSP-300, and PMS 2D-probe, and the Polar Nephelometer mounted on the research aircraft Falcon operated by Deutsches Zentrum für Luft- und Raumfahrt (DLR). All probes have different advantages and limitations, providing information about different aspects of the cloud.

The CVI probe (Ogren et al., 1985; Ström et al., 1994), which has its inlet facing the direction of flight, operates by using an internal flow opposite the flight direction to prevent ambient air and small particles to enter the probe. In the upper troposphere and at airspeeds typical of the Falcon aircraft this lower cut-off is approximately 5μm aero-

dynamic diameter. The crystals that enter the probe are evaporated and their residues are counted using condensation particle counters. A one-to-one correspondence between the residue particles and the crystals is assumed, which is proven to be a valid assumption (Seifert et al., 2003). At 1Hz data resolution one count registered by the CVI payload corresponds to an ambient crystal number density of about 0.0004 cm^{-3}.

The FSSP-300 probe use the measured response from scattered light coming from crystals illuminated by laser light (Baumgardner et al., 1992). To convert from the observed scattered light to a crystal size distribution a T-matrix calibration was used (Borrmann et al., 2000). The method yields a crystal size classification in 32 bins between 0.37 mum to 15.77 μm diameter. Due to noise in the three first channels (smallest sizes) the minimum size class starts at 0.55 μm. At 1 Hz data resolution one count registered by the FSSP-300 corresponds to a crystal number density of about 0.2 cm^{-3}.

The PMS 2D-probe classifies the size of crystals by the shadow they create when passing in front of an array of detectors illuminated by a laser. The crystals are classified in 30 bins in the size range between 25 and 800 μm diameter. Because crystals in this size range may have very irregular shapes, a number of assumptions are introduced to convert from raw data to size distributions (Gayet et al., 1993). The ambient crystal number density corresponding to one count registered by the 2D-probe depends on the crystal size, but typically the minimum detectable number density is in the range 10^{-6} cm^{-3}.

The Polar Nephelometer measures the scattering phase function of an ensemble of cloud particles in the size range from a few micrometers to about 800 μm diameter (Gayet et al., 1997). A laser beam at a wavelength of 804 nm illuminates the particles near the focal point of a paraboloidal mirror. The scattered light is detected by 44 photodiodes in angles from ±3.49 to ±169°. The direct measurement of the scattering phase function provides the means to distinguish between liquid and solid phase hydrometeors and to calculate the extinction coefficient and asymmetry parameter (Auriol et al., 2001).

Relative humidity was measured using a cryogenic frost point mirror (Ovarlez and van Velthoven, 1997). The unheated inlet, a modified Rosemount-Goodrich temperature housing, was located on the top of the fuselage. The relative humidity is determined from the Sonntag saturation vapor pressure formula (Sonntag, 1994), using the air temperature data provided by the standard instrumentation on board the Falcon. The relative uncertainty in observed relative humidity is estimated to be better than 7% (2 standard deviations).

The CPF as function of relative humidity for warm clouds is rather straightforward and the expected distribution is illustrated in Fig. 1a. The cloud form and disappear at the same relative humidity marked X_1 and X_2 in Fig. 1a. In the real world a small supersaturation, typically a fraction of a percent, is necessary to activate aerosol particles into cloud droplets. However, within measurement capabilities of relative humidity the CPF can be approximated as unity at water saturation and zero at humidities below. Solution droplets may be in equilibrium with the surrounding environment even at relative humidities well below 100%. These particles are not activated into cloud droplets in the traditional sense, but such haze clouds may still be of importance for processes in the tropopause region (Kärcher and Solomon, 1999). Ice clouds are more complicated than their liquid counterparts since they may form at one relative humidity substantially (10's of percent) above ice saturation and dissolve at a much lower humidity. The rate at which water vapor is transferred between the different phases at cold temperatures is slower than in warm clouds which is why a cirrus cloud can persist for some time in air sub-saturated with respect to ice and give rise to their often fuzzy appearance especially around cloud edges. A possible scenario is illustrated in Fig. 1b. At some humidity threshold, X_1, clouds form. At this humidity and above the CPF is one. At X_2, CPF is less than one since this point is a mixture between air parcels that have formed a cloud and where the humidity is perhaps decreasing, and air parcels that have not yet formed a cloud (i.e. reached X_1) and where the humidity might still be increasing. Once below ice saturation the cloud will eventually disappear at some humidity X_3.

3 Observations

Data analyzed in this study is limited to observations performed above 6 km altitude and temperatures below 235 K. Although different cloud-probes are based on different principles and have different detection limits, as summarized above, it is interesting to compare the consistency between probes for a subset of the data where there is an overlap in cloud detection. The FSSP-300 is able to detect clouds when crystals are smaller than the aerodynamic cut-off of the CVI, but the CVI is able to detect clouds with a much lower crystal number density than the FSSP-300 is capable of. If a subset of the FSSP-300 data is selected to emulate a CVI with respect to the size cut-off, and a subset of the CVI data is selected to emulate the FSSP-300 with respect to the number density detection limit, the two instruments should detect clouds with similar efficiency. The comparison of SH-data in Fig. 2a and of NH-data in Fig. 2b show that there is an excellent agreement between the CVI and FSSP-300 over several order in magnitude during both campaigns. Typically, the difference between the two cloud probes is in the range of percent. The CPF is plotted on a logarithmic scale to highlight the agreement even at low relative humidities. Because the physical principles are completely different the comparison in Fig. 2 proves that the two instruments perform as expected within at least the overlapping range in crystal number density and crystal size. Recall, that the CVI counts residual particles from evaporated crystals, whereas the FSSP-300 detects the scattered light from the crystals in the ambient air.

In the following we will use data from the CVI to study the presence or non-presence of clouds based on different number density thresholds, and the FSSP-300 using different crystal size thresholds. Most of the cloud water content (CWC) is located in the size range of the 2D-probe, hence we can view the data from these probes as providing information about three different aspects of cloud properties. The Polar Nephelometer observes a volume of cloudy air, that instrument provides an optical response that depends on the combined effect from both crystal size and number density.

In Figs. 3a and 3b CPF is plotted given different number density thresholds observed

by the CVI for SH and NH, respectively. For all but the highest threshold there is a sharp drop in CPF below 90% RHI. Near ice saturation some 80 to 90% of the data points exceeded a crystal number density of 0.001 cm^{-3}, whereas approximately 40% of the data points exceeded a number density of 1 cm^{-3}, and around 10% of the data points exceeded 3 cm^{-3}. It is interesting to note that there is a significant fraction of cloud observations even at very dry conditions. Both data sets show this feature, but the SH generally present higher values. It is likely that some of these data points at very dry conditions are a result of small-scale features. If the aircraft passes a cloud edge where there is a strong gradient in humidity between the interior of the cloud and the surrounding air or the investigated cloud is very patchy, a mixture of cloudy and non-cloudy air may result in clouds being detected in very dry air. Note that the typical speed of the Falcon aircraft is almost 200 $m\,s^{-1}$ and even a short instrument time response of a few seconds will smooth data over a considerable distance.

In Figs. 4a and 4b CPF is plotted given different crystal size thresholds observed by the FSSP-300 for SH and NH, respectively. The fraction of cloud data points is rather sensitive to the choice of the lower size limit. Within only a few micrometers there are some obvious differences between the two campaigns. As for the CVI data in Fig. 3, there is a marked difference in CPF above and below ice saturation. Despite the reduction in CPF below ice saturation there is still a significant fraction remaining even for the smallest particles. As for the CVI data some of these observations may be due to small-scale features. Near ice saturation clouds having a number density larger than 0.2 cm^{-3} and sizes larger than 0.55 μm were present during ca 75% of the time in the SH-campaign. In the NH this value is ca 90%. If the crystal size threshold of 1 μm is used instead, the CPF drops to 0.6 and 0.7 in the SH and NH, respectively. Hence, a very significant contribution to the CPF arrives from very small particles. Note that, in selecting the size thresholds we have used the size range available by the instruments capability and made no distinction about the type of particle, ice crystal, haze droplet, or any other class of particle. Simply size has been used to classify the particles.

In Figs. 5a and 5b CPF is plotted for the presence of clouds defined as having crys-

tals larger than 25 μm or larger than 100 μm diameter as observed by the 2D-probe during the SH- and NH-campaign, respectively. The two curves are essentially on top of each other, which indicate that whenever 25 μm crystals are present in the cloud crystals of 100 μm diameter are present as well. The distributions in Fig. 5 share many features seen in Figs. 3 and 4. As for the other two probes the drop in CPF below the saturation level is located around 90% rather than 100% RHI. It is not clear if this characteristic is a result of smoothing in the data as mentioned above or any other problems in the observations, or if the ambient humidity actually must decrease to below 90% in order for any significant evaporation to take place. If ventilation around the crystals is impeded or insufficient for some reason it is possible that the microclimate surrounding the crystals is quite different from the macroclimate measured by the sensors on the aircraft. This could result in the near field humidity being different than the far field humidity. Rapid changes in humidity due to wave motion could also be a cause for the presence of clouds in seemingly very dry environments if the time-scale for the cloud particles to adjust to the new condition is longer than the time-scale of changes in ambient humidity.

In Fig. 6, cloud data points are defined as having an extinction coefficient of 0.05 km^{-1} or larger as measured by the Polar Nephelometer. In addition, this criterion had to be fulfilled during at least four consecutive seconds in order to be considered an in-cloud data point. A microphysical equivalent of this optical threshold corresponds to crystals of 5 μm diameter at a number density of roughly between 0.05 and 0.1 cm^{-3}. The criteria used to define Polar Nephelometer in-cloud data points presented in Fig. 6 are the same as used by Ovarlez et al. (2002). Whereas the CPF in Figs. 3, 4, and 5 were calculated for each percent of relative humidity the Polar Nephelometer data is average over a 10% range. Clearly the CPF in the NH data reach unity at a lower humidity. In the sub-saturated region the NH CPF have more or less disappeared around 70% RHI, whereas clouds in the SH are still present during almost ten percent of the time at humidities down to 40% RHI. Near ice saturation clouds are present at almost the same fraction of the time, with possibly a slightly higher fraction in the SH-data. Be-

tween ice saturation and the humidity where CPF reach unity, the two data sets display a noticeable minimum. This feature can also be traced in the data of the other probes presented in Figs. 3, 4, and 5, but the extent of the minimum depends on the threshold used to characterize in-cloud and out-of-cloud data points. We will focus more on this feature below.

4 Interpretation of CPF as function of relative humidity

As was outlined in the scenario presented in Fig. 1b, the CPF will be less than unity at the ice saturation level because clouds at cold temperatures form at ice supersaturated conditions. In terms of the ice saturation ratio $S = (RHI/100\%)$, we can define the cloud presence fraction as the ratio between two probabilities

$$\mathrm{CPF} = \frac{P(S_c)}{P(S)}. \tag{1}$$

$P(S)$ is the probability that an air parcel reach above a given ice saturation ratio S, and $P(S_C)$ the probability that an air parcel reach above a critical ice saturation ratio S_C, where $1/eS \leq S_C$. By definition, CPF is unity whenever $S > S_C$. Kärcher and Haag, (2003) has shown that the probability to find a parcel of air supersaturated with respect to ice decreases monotonously with increasing values of S and can be approximated well by an exponential decrease of the form:

$$p(S) = C \exp\left[\frac{-S}{S_0}\right], \; S \geq 1, \tag{2}$$

where C is a normalization constant and S_0 a scaling parameter. From Eq. (2) we can write

$$P(S_C) = C \int_{S_C}^{\infty} \exp\left[\frac{-S_C}{S_0}\right] dS = C\, S_0 \exp\left[\frac{-S_C}{S_0}\right]; \tag{3}$$

$$P(S) = C \int_{S}^{\infty} \exp\left[\frac{-S}{S_0}\right] dS = C\, S_0 \exp\left[\frac{-S}{S_0}\right]; \tag{4}$$

Equations (3) and (4) give the probability to find an air parcel above a saturation ratio S and S_C, respectively. Thus the cloud presence fraction is given by,

$$\mathrm{CPF} = \exp\left[\frac{S - S_C}{S_0}\right] \quad : \quad (1 \leq S \leq S_C). \tag{5}$$

If clouds form at S_C, the cloud presence fraction at any $S(1 \leq S \leq S_C)$ is given by Eq. (5), provided that the probability distributions can be described by the exponential function as in Eq. (2) and an appropriate value of S_0 is used. Equation (2) may be used to approximate the probability distribution of saturation ratios observed during the INCA campaigns (Ovarlez et al., 2002). The probability distribution to use (read value of S_0) is not the observed distribution, but rather the distribution in the absence of cloud formation. However, the above simple model contains important simplifications. The vertical wind field in the absence of clouds, the interaction of water vapor with cloud particles after cloud formation, and mixing processes influence the probability to observe a certain value of S, and this influence cannot be easily accounted for.

Once a cloud has formed in an air parcel the growing ice crystals will prevent the humidity to reach the saturation ratio it could have attained in the absence of clouds. The uptake of water vapor by the crystals will subsequently reduce the humidity back down to ice saturation. Thus, clouds influence the distribution of relative humidity by changing its slope and hence the value of S_0. These processes along with dynamical factors have been discussed in detail by Haag et al. (2003) based on the INCA measurements of relative humidity.

Further, the probability functions used to calculate the CPF in Eq. (5) do not explicitly take into account any effect on the CPF caused by precipitation or mixing from entrainment and detrainment. To fully examine this issue detailed three dimensional

cloud-resolving simulations must be carried out, but we can briefly discuss some possible implications. Obviously, mixing between two air parcels with similar properties in term of microphysics and relative humidity will not have any large impact on the observed CPF. The larger the difference between the air parcels the more the mixing processes will influence the end result. We can thus expect the largest influence from mixing to occur near cloud edges. If mixing between cloudy and non-cloudy air results in a larger volume of cloudy air than the volume of the original cloudy air parcel the net effect is an enhanced CPF around ice saturation. Mixing processes simply generates cloudy air which otherwise would not exist.

Enhancements of the CPF near the ice saturation seen in Figs. 4 and 5 in, particular the SH data, could be indicative of cloud edge mixing. Although the measurement flights did not directly intend to fly at cloud edges the strategy used of approaching the cloud from above, may have caused an over representation of the upper parts of cirrus clouds compared to an entirely random sampling. However, the fraction of measurements performed at cloud edges should be put in relation to the total amount of measurements. As discussed in the text above cloud edges may be responsible for some of the cloud observations at very low relative humidities due to the averaging effect of an aircraft flying at almost 200 m s^{-1}. One aspect that might complicate things is if mixing is part of the cloud formation process as for instance during turbulent mixing near jet winds or breaking waves. How much of the cloudy volume that results from such processes is not known. Precipitation would be expected to make the largest impact in sub saturated air since precipitation within the cloud will only have a marginal effect on the CPF. Recall that the besides the Nephelometer the thresholds where defined as at least fulfilling a number density or size criteria.

In summary, we use the value $S_0 = 2$ as an empirical subjectively best fit parameter and vary S_{cr} to obtain a set of CPF curves plotted in Figs. 7, 8, and 9 along with the CPF derived from the measurements. In the following we will compare data from the two campaigns.

5 Comparing the cloud presence fractions from the SH and NH campaigns

Several of the different thresholds presented in Figs. 3, 4, 5, and 6 present a CPF distribution that is roughly consistent to Eq. (5) if using $S_0 = 2$. In Figs. 7, 8, and 9 below, the calculated CPF have been overlaid for different critical saturation ratios S_C, in steps of 0.1.

In Fig. 7a observed CPF in the SH and NH are compared for a CVI threshold of 0.001 cm^{-3}. As for the Polar Nephelometer data in Fig. 6, the NH CPF reach unity at a lower saturation compared to the SH, with a difference of approximately 0.2 to 0.25. The SH CPF follows the calculated value fairly well from saturation up to about $S = 1.45$, where there is a very significant drop in observed CPF. The general trend in the decrease of the NH CPF between $S = 1.3$ and $S = 1$ agrees fairly well but the details are not. To emphasize what we mean with fairly well, the endpoints where the observations intersect with the calculated slopes are marked with black and red symbols. With the exception of the deep minimum shown in the SH data, the observations wiggles around the calculated slop. The NH data systematically stay below the calculated slope. The trend, defined by the endpoints, is in agreement with the calculated slope.

The CVI samples particles larger than a certain aerodynamic size and the instrument will not register any counts unless the crystals grow to this lower cut-off size. At the point when clouds form and shortly thereafter some (probably most) of the ice crystals are too small to be detected by the CVI. This would result in the CPF being underestimated at the relative humidities where clouds form. The same reasoning can be applied to the other probes, which provides an explanation for the distinct minima observed in the Polar Nephelometer data presented in Fig. 6. Thus, the interpretation of the local minimum in observed CPF above ice saturation is that it represents the humidity range where clouds preferentially form. Considering the typical temperatures observed during the experiment (around −47°C), the CPF minimum around $S = 1.45$ in the SH is slightly lower than the equilibrium homogeneous freezing threshold at this

temperature (Koop et al. 2000). Using an analogous interpretation for the NH suggests that clouds form preferentially at saturation ratios below 1.3, which would suggest that the mode of nucleation was different during the respective campaigns.

In Fig. 7b observed CPF in the SH and NH are compared for a CVI threshold of 1 cm^{-3}. As for the lower threshold the NH CPF reaches unity at a lower saturation ratios compared to the SH. The local minimum for the SH is not as evident as in Fig. 7a but can be traced by comparing with Fig. 4a where the different thresholds where plotted together for the same data set. Likewise, a local minimum between approximately 1.15 and 1.30 for the NH can be traced back when comparing with Fig. 4b, where the minimum is most evident for the threshold of 0.3 cm^{-3}. The different data sets in Figs. 7a and 7b reach unity between 1.3 and 1.6, but if the modeled distributions are traced back to unity, illustrated by an arrow in Fig. 7b, the corresponding Sc will be in the range 2.7 to 2.9. These saturation ratios are significantly above the saturation level for liquid water and are unlikely to occur in the atmosphere. The interpretation of these very high values is that they are not what is necessary to form the cloud in terms of a critical value, but represents the excess water vapor required to grow the crystals to a detectable size. In the case of Fig. 7b this corresponds to enough available water to grow crystals with a number density of at least 1 cm^{-3} to at least 4 to 5 μm diameter. An example would be an ascending parcel of air that first reach the critical saturation ratio to form a cloud, in the range 1.3 to 1.6, but it continues to ascend until it reaches conditions that in the absence of clouds would have generated a saturation ratio of between 2.7 and 2.9. The amount of water vapor responsible for creating a super saturation of 1.7 or 1.9 times the amount of water vapor available at ice saturation corresponds to the adiabatic cloud water content.

In Figs. 8a and 8b the SH and NH data are compared for particle size thresholds 0.55 μm and 1 μm diameter. In relation to Fig. 7 the FSSP thresholds show a larger differences between the SH and NH data. The local minimum in the SH CPF is evident, and as for the CVI and Polar Nephelometer thresholds the NH CPF become unity at lower saturation ratios compared to the SH CPF. In Fig. 8a the observed trend,

indicated by the markers, does not fit the calculated trend very well. In Fig. 8b the observed and modeled trends appear to agree more, but the NH data is sometimes very much below the calculated distribution. The SH data better follows the calculated lines as indicated in the figures, again with the exception of the distinct minima. Clouds where the particles are only between 0.55 μm and 1 μm diameter are present at a relatively large fraction of the time. This is true during both campaigns, but with a slightly lower fraction in the SH at ca 15% compared to 20% in the NH.

The appearance of ice crystals at moderate subsaturations ($S \sim 0.8$) could be explained by the time needed to fully evaporate water from large crystals, but the large CPF at considerable drier ambient conditions is difficult to explain. The fact that these small particles clearly respond to changes in humidity prove that they are mainly made up of water and we can exclude the possibility that they are simply surface derived debris such as mineral dust or ash from fire plumes etc. However, we do not know for sure that they are ice. The Polar Nephelometer did not observe liquid water at temperatures below −34°C. Nevertheless, this does not exclude that these small particles are made of liquid water since the optical response from an ensemble of these small particles may be less than the detection limit of the Polar Nephelometer. To detect liquid water (spherical particles) given micron size particles would require a number density of several 10's per cubic centimeter.

The presence of clouds at very dry ambient condition has previously been reported by Ström and Heintzenberg (1994). Satellite imagery suggested that the investigated cloud formed in the outflow from a cumulonimbus cloud. This air is significantly affected by recent transport of boundary layer air, which may contain a relatively large fraction of pollutants compared to the rest of the tropopause region. If and to what extent pollutants scavenged by the crystals may influence the thermodynamic properties of ice crystals is not well understood. However, the study by Seifert et al. (2003) indicates that with increasing interstitial aerosol number density the average relative humidity required for clouds to dissolve is decreasing.

In Fig. 9, the SH and NH data are compared for a crystal size threshold of 25 μm

as measured by the PMS-2D probe. As for the number density threshold presented in Fig. 7b the two data sets are difficult to separate at saturation ratios below 1.3. Above this saturation level the difference is significant. The NH-data reach unity around $S = 1.4$, whereas the SH-data really never reaches unity in our data. The observed differences at high RHI could be explained by the clouds forming at a lower RHI in the NH, which would simply give the crystals more time to grow. Once the humidity falls back to ice saturation enough time have elapsed making the initial lead-time unimportant. It should also be pointed out that the amount of data drastically decreases with increasing relative humidity. Compared to the CVI and FSSP data presented in the figures above, PMS 2D data show more variability. At ice saturation the calculated CPF represents the probability or fraction of air parcels that reached, or would have reached in the case of a cloud free atmosphere, a critical ice saturation level. As pointed out above the difference between ice saturation and the critical saturation ratio corresponds to the adiabatic cloud water content. By differentiating between successively calculated CPF at ice saturation a calculated cloud water content distribution can be derived. Normalizing the distribution with the CWC increments gives a probability function. The derived function is plotted in Fig. 10a together with the observed CWC distributions from the SH and NH campaigns. The observed cloud water content is taken as the sum of the CWC's measured by the 2D-probe using an empirical formulation (Gayet et al., 2002) to convert from size distribution to CWC, and the CWC derived from the FSSP- 300 size distribution assuming spherical particles using a particle density of $0.9\,\mathrm{g\,cm^{-3}}$. The observed distributions are normalized to their integral values from $0.01\,\mathrm{mg\,m^{-3}}$ and higher, which makes the areas under the curves equal to unity and comparable to the derived distribution. Because a given relative humidity will correspond to different absolute water contents depending on the ambient temperature, the derived distribution has been shifted to match the observed CWC distribution of the SH. We are interested in the CWC at the point when the humidity have relaxed back down to the saturation level, and only data between 95% and 105% RHI was included in the distribution of observed data.

The observed and calculated distributions presented in Fig. 10a show some interesting features. There is a striking similarity between the modeled and observed distributions. The calculated distribution (blue line in Fig. 10a) predicts a mode covering a range of cloud water contents ranging over approximately two orders of magnitude. The distribution is skewed with a tail towards lower CWC's. Much of this is seen in the observed distribution as well. However, the calculated distribution does not capture the increased observation density below $0.01\,\mathrm{mg\,m^{-3}}$. These data points are almost entirely data from the FSSP-300 when the 2D-probe did not register any crystals. It is also interesting to note that the two data sets are rather similar, which gives some confidence that the data sets make up a representative statistical ensemble.

Adjusting the calculated CWC distribution to match the observed distribution in Fig. 10a, is the same as fixing a water vapor content to the ice saturation level. In the example presented in Fig. 10a, ice saturation corresponds to a water vapor content of $8\,\mathrm{mg\,m^{-3}}$. However, the saturation water vapor content at the typical temperatures around -47°C is $\sim 55\,\mathrm{mg\,m^{-3}}$, which is significantly higher. Assuming adiabatic processes, there is potentially much more water available than what is observed in the cloud based on the temperature. This apparent difference would be smaller if clouds formed and grew at temperatures colder than the typical temperature. Whether clouds preferentially form via wave motion or semi-continuous uplift would also influence the comparison between CWC and ambient temperature. To quantify the net effect require numerical simulations and will be a study of its own. Nonetheless, in the latter case the saturation would always be reached at altitudes below the reference altitude corresponding to higher temperatures, whereas in the case that clouds are formed in waves saturation could be reached either above or below the observed altitude. The adiabatic model does not consider mixing between cloudy and non-cloudy air, which would result in a lower mean CWC. This is probably the main mechanism to reduce the CWC in non-precipitating clouds, but something we know very little about in cirrus clouds. Diabatic warming in the cloud could also explain some of the difference observed. The calculated geometric mean CWC in Fig. 10a is 7.3 and $10.4\,\mathrm{mg\,m^{-3}}$ for the SH and

NH, respectively. Note that changing the water vapor content corresponding to ice saturation do not change the form of the calculated distribution, only the location of the mode. Figure 10b shows the same as Fig. 10a, but data only represents the temperature range between −47°C and −48°C. No dramatic difference can be seen between the two figures other than the absence of the very low cloud water contents and more jagged appearance in Fig. 10b due to less data. The blue derived distribution is the same in both figures.

6 Summary and conclusion

In this study we have made use of different sensors to determine the presence or non-presence of cirrus clouds as function of relative humidity over ice. For a given observed relative humidity above ice saturation the cloud presence fraction (CPF) tends to be higher in the NH-data compared to SH-data. A significant CPF is also observed for very dry conditions well below ice saturation. This mainly concerns particles of a few micrometer in diameter and at low number densities ($< 0.03\,\mathrm{cm}^{-3}$). While the appearance of ice crystals at moderate subsaturations (∼80%) could be explained by kinetic limitations when ice particles evaporate, observations at lower humidities require further investigations.

The distribution of CPF as function of relative humidity presents a distinct local minimum between 140% and 155% RHI in the SH-data. A less pronounced local minimum in CPF is also suggested in the NH-data between approximately 115% and 130% RHI. Our interpretation of these features is that they correspond to the preferred ice nucleation thresholds during respective campaigns. The SH threshold is consistent with homogeneous freezing, whereas the NH threshold would indicate heterogeneous ice formation.

The distribution of CPF as function of relative humidity, decreasing from unity at high humidities above the cloud particle nucleation threshold to smaller values around ice saturation, can be understood assuming a simple relation describing the probability of

reaching successively higher humidities in an air parcel. The probability distribution used to explain the observations depends on the dynamical forcing of the air parcels induced by the vertical wind field and the microphysical interaction between water vapor and ice crystals.

The difference between the peak relative humidity that would potentially occur in a cloud-free atmosphere and ice saturation corresponds to the adiabatic cloud water content. The shape of the CWC distribution derived from the probability function agrees well the shape of the observed CWC distribution. However, based on the typical temperatures during the two experiments, the expected CWC calculated from the probability distributions is significantly higher than what was observed.

This study and the study by Haag et al. (2003) strongly suggest that ice formation occur at different humidity thresholds in the Southern and Northern Hemisphere midlatitudes. Although the data is limited to two field campaigns (currently the only analysis that include in-situ data from the midlatitude Southern Hemisphere), the differences between the campaigns are clear and observed by all the cloud probes.

The presence of small micrometer sized particles observed in both campaigns, but predominantly in the NH, is puzzling. In dry environments these could be remnants from larger crystals that evaporate, but the small particles appear to be almost ubiquitous and present at all humidities. Clearly the analysis shows that there is a need for a device that has the crystal size detection of the FSSP-300 and number density sensitivity of the CVI.

Acknowledgements. This work was funded by the European Commission through the projects INCA and PARTS. It also contributes to the project “Particles and Cirrus Clouds” (PAZI) supported by the Helmholtz-Gemeinschaft Deutscher Forschungszentren (HGF). The Swedish Research Council is sponsoring this work by supporting ITM in airborne aerosol and cirrus activities. Thanks to the entire INCA team for help in collecting the data and to K. Gierens for discussions regarding the probability distributions of relative humidity.

References

Auriol, F., Gayet, J. F., Febvre, G., Jourdan, O., Labonnotte, L., and Brogniez, G.: In situ observations of cirrus cloud scattering phase function with 22° and 46° halos: Cloud field study on 19 February 1998, J. Atmos. Sci., 58, 3376–3390, 2000.

Baumgardner, D., Dye, J. E., Gandrud, B. W., and Knollenberg, R. G.: Interpretation of measurements made by the forward scattering spectrometer probe (FSSP-300) during the Airborne Arctic Stratospheric Expedition, J. Geophys. Res., 97, 8035–8046, 1992.

Borrmann, S., Luo, B. P., and Mishchenko, M.: Application of the T-matrix method to the measurement of aspherical (ellipsoidal) particles with forward scattering optical particle counters, J. Aerosol Sci., 31, 789–799, 2000.

Boucher, O.: Air traffic may increase cirrus cloudiness, Nature, 397, 30–31, 1999.

European Commission: European research in the stratosphere 1996–2000, Second assessment on stratospheric research. G. T. Amanatidis and N. R. P. Harris (Eds.), 378, 257–307, 2002.

Gayet, J. F., Brown, P. R., and Albers, F.: A comparison on in-cloud measurements obtained with six PMS 2D-C probes, J. Atmos. Ocean. Tech., 10, 180–194, 1993.

Gayet, J. F., Crépel, O., Fournol, J. F., and Oshchepkov, S.: A new airborne Polar Nephelometer for the measurements of optical and microphysical cloud properties. Part I: Theoretical design, Ann. Geophysicae, 15, 451–459, 1997.

Gayet, J.-F., Auriol, F., Minikin, A., Ström, J., Seifert, M., Krejci, R., Petzold, A., Febvre, G., and Schumann, U.: Quantitative measurement of the microphysical and optical properties of cirrus clouds with four different in situ probes: Evidence of small ice crystals, Geophys. Res. Lett., 29, 14342-14 346, 2002.

Haag, W., Kärcher, B., Ström, J., Minikin, A., Lohmann, U., Ovarlez, J., and Stohl, A.: Freezing thresholds and cirrus cloud formation mechanisms inferred from in situ measurements of relative humidity, Atmos. Chem. Phys. Discuss., 3, 3267–3299, 2003.

Intergovernmental Panel on Climate Change (IPCC), 1999: Aviation and the Global Atmosphere (Penner, J. E., Lister, D. H., Griggs, D. J., Dokken, D. J., and McFarland, M. eds.), 373, Cambridge Univ. Press, Cambridge, UK, 1999.

Kristensson, A., Gayet, J. F., Ström, J., and Auriol, F.: In situ observations of a reduction in effective crystal diameter in cirrus clouds near flight corridors, Geophys. Res. Lett., 27, 681–684, 2000.

Kärcher, B. and Lohmann, U.: A parameterization of cirrus cloud formation: Homogeneous freezing of supercooled aerosols including effects of aerosol size, J. Geophys. Res., 107, 4698, 10.1029/2001JD001429, 2002.

Kärcher, B. and Solomon, S.: On the composition and optical extinction of particles in the tropopause region, J. Geophys. Res. 104, 27 441–27 459, 1999.

Kärcher, B. and Lohmann, U.: A parameterization of cirrus cloud formation: Heterogeneous freezing, J. Geophys. Res., 108, 10.1029/JD2002003220, in press, 2003.

Kärcher, B. and Ström, J.: The roles of dynamical variability and aerosols in cirrus cloud formation, Atmos. Chem. Phys. Discuss., 3, 1415–1451, 2003.

Kärcher, B. and Haag, W.: Factors controlling upper tropospheric relative humidity, submitted manuscript, 2003.

Koop, T., Luo, B. P., Tsias, A., and Peter, T.: Water activity as the determinant for homogeneous ice nucleation in aqueous solutions, Nature, 406, 611–614, 2000.

Lohmann, U. and Kärcher, B.: First interactive simulations of cirrus clouds formed by homogeneous freezing in the ECHAM general circulation model, J. Geophys. Res., 107, 4105, 10.1029/2001JD000767, 2002.

Mannstein, M., Meyer, R., and Wendling, P.: Operational detection of contrails from NOAA-AVHRR-data, Int. J. Remote Sensing, 20, 1641–1660, 1999.

Meyer, R., Mannstein, H., Meerkötter, R., Schumann, U., and Wendling, P.: Regional radiative forcing by line-shaped contrails derived from satellite data, J. Geophys. Res., 107, 10.1029/2001JD000426, 2002.

Ogren, J. A., Heintzenberg, J., and Charlson, R. J.: In-situ sampling of clouds with a droplet to aerosol converter, Geophys. Res. Lett., 12,121–203, 1985.

Ovarlez, J. and van Velthoven, P.: Comparison of water vapor measurements with data retrieved from ECMWF analyses during POLINAT experiment, J. of Appl. Meteorol., 1329–1335, 1997.

Ovarlez, J., van Velthoven, P., Sachse, G., Vay, S., Schlager, H., and Ovarlez, H.: Comparison of water vapor measurements from POLINAT 2 with ECMWF analyses in high-humidity conditions, J. Geophys. Res., 105, 3737–3744, 2000.

Ovarlez, J., Gayet, J.F., Gierens, K., Ström, J., Ovarlez, H., Auriol, F., Busen, R., and Schumann, U.: Water vapour measurements inside cirrus clouds in Northern and Southern hemispheres during INCA, Geophys. Res. Lett., 29, 1813–1817, 2002.

Seifert, M., Ström, J., Krejci, R., Minikin, A., Petzold, A., Gayet, J.-F., Schumann, U., and Ovar-

lez, J.: In situ observations of aerosol particles remaining from evaporated cirrus crystals: Comparing clean and polluted air masses, Atmos. Chem. Phys. Discuss., 2, 1599–1633, 2002.

Seifert, M., Ström, J., Krejci, R., Minikin, A., Petzold, A., Gayet, J.-F., Schlager, H., Ziereis, H., Schumann, U., and Ovarlez, J.: Aerosol-cirrus interactions: A number based phenomenon at all?, submitted to Atmos. Chem. Phys. Discuss., 2003.

Sonntag, D.: Advancements in the field of hygrometry, Meteorol. Z., 3, 51–66, 1994.

Ström, J. and Heintzenberg, J.: Water-Vapor, Condensed Water, and Crystal Concentration in Orographically Influenced Cirrus Clouds, J. Atmos. Sci., 51, 2368–2383, 1994.

Ström, J., Heintzenberg, J., Noone, K. J., Noone, K. B., Ogren, J. A., Albers, F., and Quante, M.: Small crystals in cirrus clouds: their residue size distribution, cloud water content, and related cloud properties, J. Atmos. Res., 32, 125–141, 1994.

Ström, J. and Ohlsson, S.: In situ measurements of enhanced crystal number densities in cirrus clouds caused by aircraft exhaust, J. Geophys. Res., 103, 11 355–11 361, 1998.

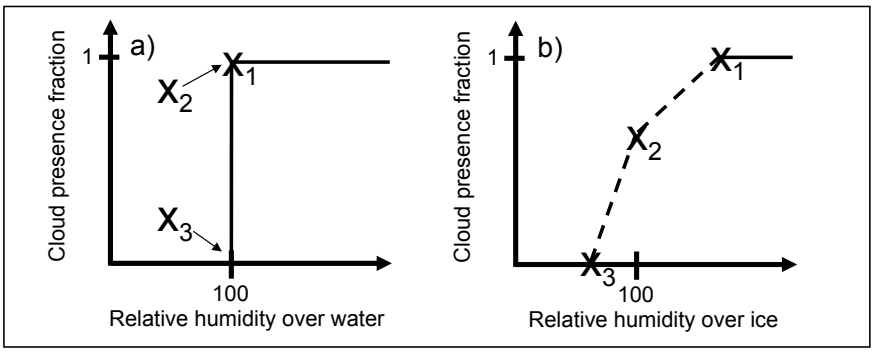

Fig. 1. Schematic illustration of the cloud presence fraction (CPF) as function of relative humidity for liquid clouds **(a)**, and ice clouds **(b)**. The relative humidity where clouds form is marked X_1 and the point where clouds start to dissolve is marked X_2. The point where the cloud has completely disappeared is marked X_3.

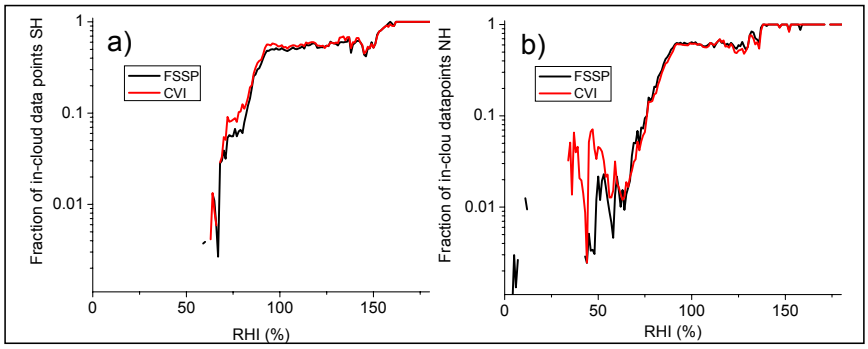

Fig. 2. Cloud presence fraction as function of relative humidity over ice using similar detection thresholds for the two probes with respect to crystal size ($> 4\,\mu$m) and crystal number density ($> 0.3\,\mathrm{cm}^{-3}$). Data from SH **(a)** and from NH **(b)**.

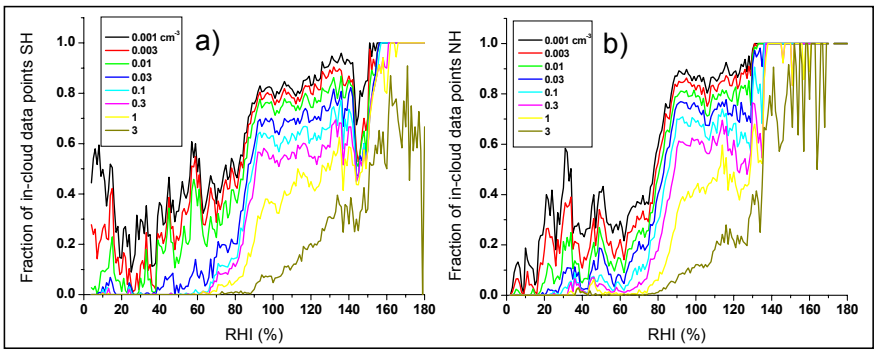

Fig. 3. Cloud presence fraction as function of relative humidity over ice for different crystal number density thresholds as measured by the CVI. If the probe, at a given RHI, observes a number density equal to or larger than the indicated thresholds found in the figure labels the data point is considered a cloudy data point. Data from SH **(a)** and from NH **(b)**.

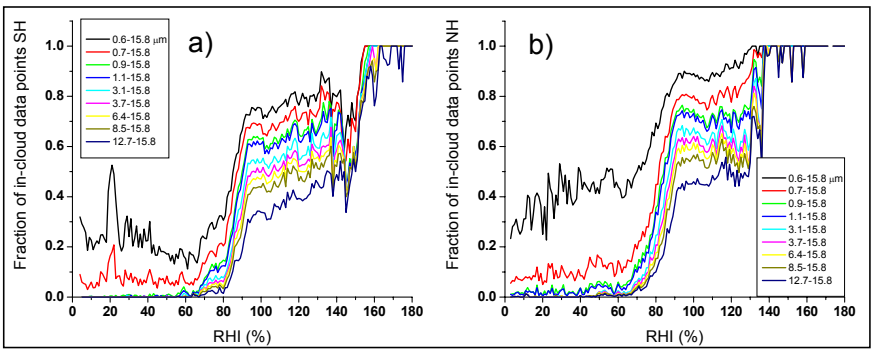

Fig. 4. Cloud presence fraction as function of relative humidity over ice for different crystal size thresholds as measured by the FSSP-300. If the probe, at a given RHI, observes any crystals having a size equal to or larger than the indicated thresholds found in the figure labels the data point is considered a cloudy data point. Data from SH **(a)** and from NH **(b)**.

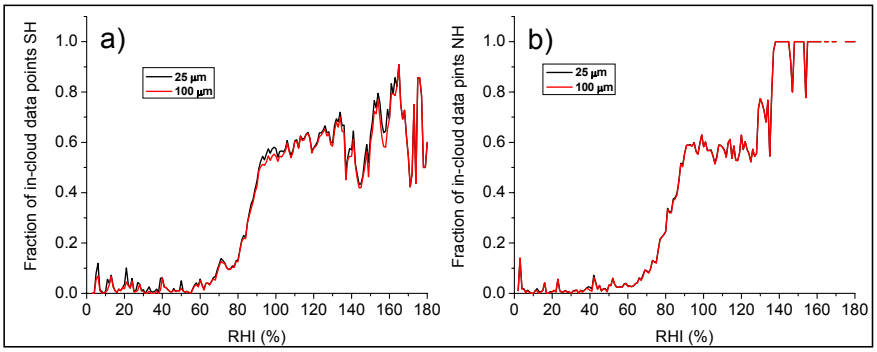

Fig. 5. Cloud presence fraction as function of relative humidity over ice for different crystal size thresholds as measured by the PMS-2D probe. If the probe, at a given RHI, observes any crystals having a size equal to or larger than the indicated thresholds found in the figure labels the data point is considered a cloudy data point. Data from SH **(a)** and from NH **(b)**. Note that in Fig. 5b the black line, representing the 25 μm threshold, is covered by the red line.

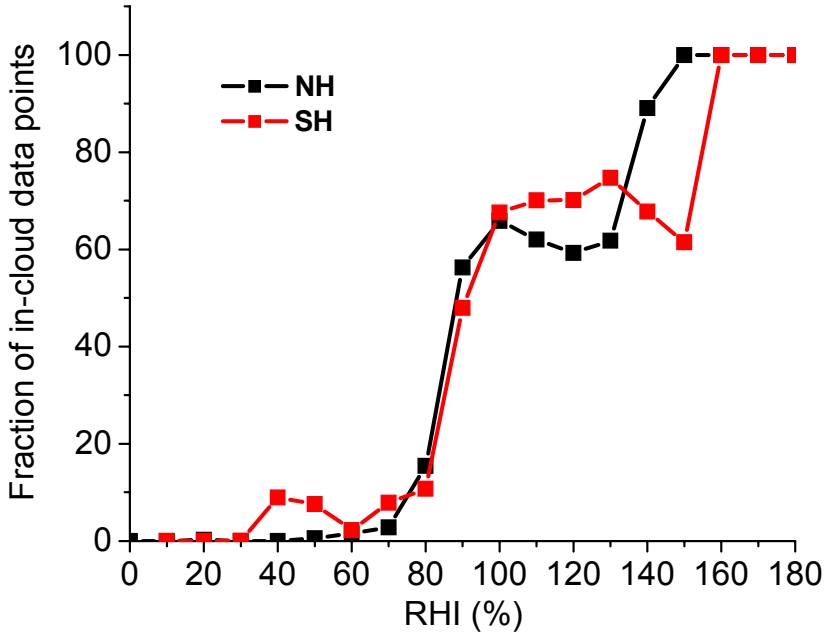

Fig. 6. Cloud presence fraction as a function of relative humidity over ice measured by the Polar Nephelometer. If the probe, at a given RHI, observes an extinction coefficient exceeding 0.05 km^{-1} during four consecutive seconds the data point is considered a cloudy data point. Only data during straight and level flight segments are included.

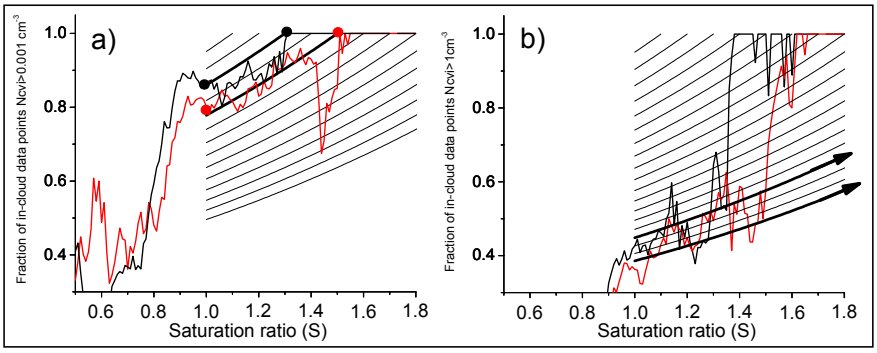

Fig. 7. Comparison of the cloud presence fraction observed in the SH and NH campaigns for same CVI number density thresholds, 0.001 cm^{-3} **(a)** and 1 cm^{-3} **(b)**. The thin lines are calculated distributions of CPF based on equation 5 and using S_0 = 2. Lines that link the points where data intercepts ice saturation and where the CPF becomes unity are highlighted. If these points are within the domain of the plot they are marked with black and red symbols to emphasize the trend, otherwise arrows indicate a range of possible lines leading to saturation ratios outside of the plot.

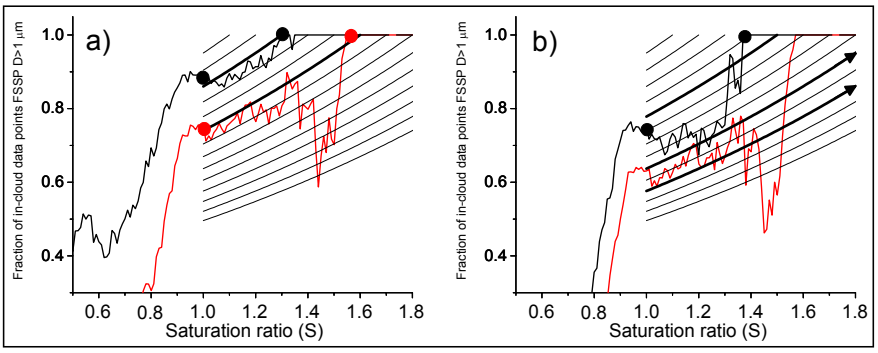

Fig. 8. Comparison of the cloud presence fraction observed in the SH and NH campaigns for same FSSP-300 threshold diameters, 0.5μm **(a)** and 1 μm **(b)**. The thin lines are calculated distributions of CPF based on Eq. (5) and using S_0 = 2. Arrows and markers as in Fig. 7.

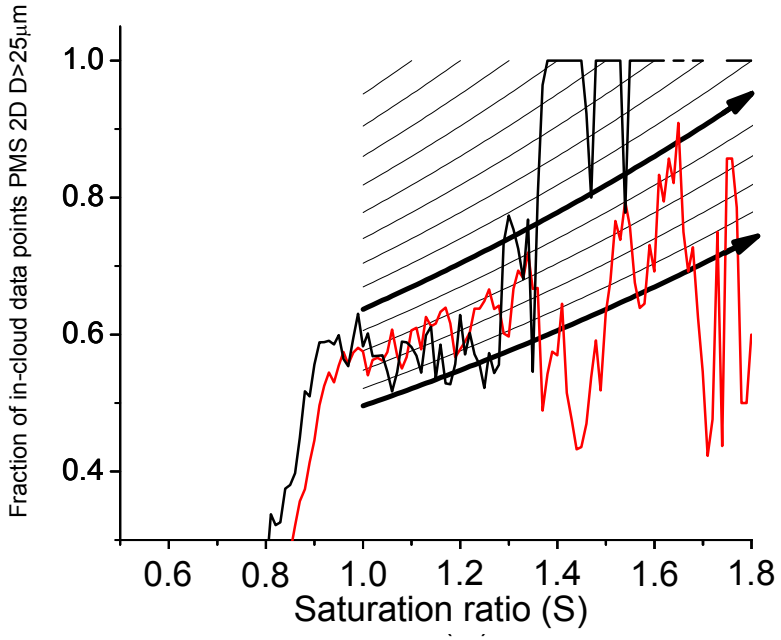

Fig. 9. Comparison of the cloud presence fraction observed in the SH and NH campaigns for same PMS-2D threshold diameters of 25 μm. Using a threshold of 100 μm yields essentially the same figure c.f. Figs. 5a and 5b. The thin lines are modeled distributions of CPF based on equation 5 and using S_0 = 2. Arrows are as in Fig. 8.

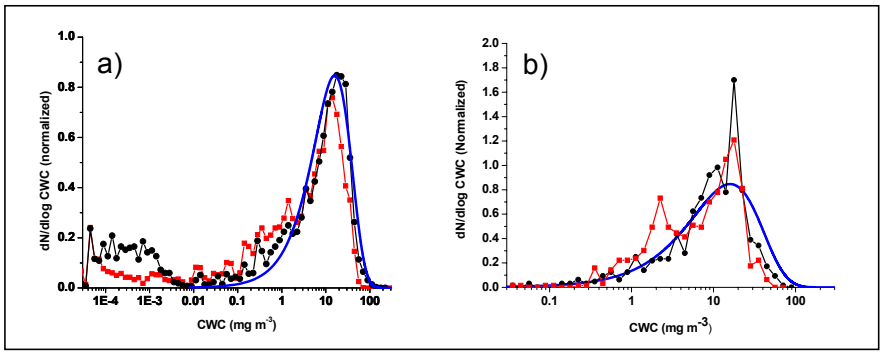

Fig. 10. Comparison between the observed distributions of cloud water content (SH red symbols and NH black symbols) and the distributions derived by using Eq. (5) and S_0 = 2 (blue line). In **(a)** all temperatures below 235 K and relative humidities between 95 and 105% RHI are used. In **(b)** the temperature only ranges between 225 and 227 K. The observed CWC is based on the sum of the FSSP-300 and 2D-probe. The derived distribution (blue line) is the same in both plots. Note the different axis scales.